ELSEVIER

Journal of Electroanalytical Chemistry 428 (1997) 25–32

JOURNAL OF ELECTROANALYTICAL CHEMISTRY

Investigation of the potential distribution in porous nanocrystalline TiO_2 electrodes by electrolyte electroreflection

G.K. Boschloo, A. Goossens *, J. Schoonman

Laboratory for Applied Inorganic Chemistry, Delft University of Technology, Julianalaan 136, 2628 BL Delft, Netherlands

Received 16 October 1996; revised 2 January 1997

Abstract

In order to investigate the potential distribution in porous nanocrystalline TiO_2 electrodes, an electrolyte electroreflection (EER) study has been undertaken. With front-side illumination a weak featureless sub-bandgap EER response is obtained due to surface states present at the TiO_2|electrolyte interface. Back-side illumination (through the indium tin oxide (ITO) coated glass support) results in EER spectra with a clear feature in the bandgap region, probably due to electric field modulation in TiO_2 particles located at the ITO|TiO_2 interface. In indifferent aqueous electrolyte, steady-state photocurrent generation in porous nanocrystalline TiO_2 electrodes is essentially independent of the applied potential. Polarising the nanoporous electrode close to the flat-band potential results in filling of surface states, which causes marked effects on the front- and back-side EER signals as well as on the alternating-photocurrent response. Surface states are located ca. 0.4 eV below the conduction band edge of TiO_2. © 1997 Elsevier Science S.A.

Keywords: TiO_2 electrodes; Porous nanocrystalline electrodes; Electrolyte electroreflection; Potential distribution

1. Introduction

Porous nanocrystalline metal oxide electrodes have a great potential for many applications, such as dye-sensitised photoelectrochemical solar cells [1–3], electrochromic windows [4–6], and lithium ion batteries [7]. Nanostructured electrodes are composed of typically 5 to 50 nm-sized particles, which are partly sintered together to form a mechanically stable porous film. The surface area of these films is much larger than the geometrical area. For example, 1 cm^2 of a 5 μm thick film of nanostructured TiO_2, comprising primary particles of 20 nm diameter, may have an actual surface area of about 750 cm^2. The high surface-to-volume ratio as well as the very small particle size provide nanostructured electrodes with unique electronic and optical properties.

In spite of the great interest in nanostructured metal oxide electrodes, little is known of the electric potential distribution and charge transport mechanisms in this type of electrode. In contrast, for single-crystalline and polycrystalline semiconductor electrodes these properties are well established [8,9]. In the latter types of electrode, generally a Schottky-barrier is formed at the semiconductor|electrolyte interface. In a region near the interface of the semiconductor, the valence and conduction bands are bent, and the semiconductor is depleted of free charge carriers, i.e. the so-called space charge or depletion layer. Under depletion conditions, there is an electric field in this layer which effectively separates light-generated electron–hole pairs. In porous nanocrystalline electrodes, however, no significant potential drop seems to be present between the centre and the surface of an individual semiconductor particle, due to the very small particle size in combination with a low donor density [2]. Nevertheless, it has been demonstrated that efficient photocurrent generation can still take place in this type of electrode, which is explained by the efficient capture of the photoholes by redox species in the solution [10]. In contrast to dense macroscopic semiconductor electrodes, most efficient photo-induced charge separation in porous nanocrystalline electrodes takes place close to the conductive support [10–13]. Södergren et al. [12] have derived a model in which transport of photo-generated electrons in the nanoporous film is driven by diffusion only. Despite the simplicity of this model, simulations for the spectral photocurrent response of nanoporous TiO_2 electrodes are in

* Corresponding author. E-mail: a.goossens@stm.tudelft.nl.

PII S0022-0728(97)00037-5

good agreement with the experimental data. The influence of the applied voltage has been introduced into this model by taking into account that the electron concentration in the conductive support is determined by the applied voltage [12,13]. It seems unrealistic, however, that no electric field inside the nanoporous semiconductor film exists when differences in electron concentrations are present, or when external voltages are applied. Some studies report on the enhancement of the incident photon-to-current conversion efficiency (IPCE) when higher positive voltages are applied to porous n-type metal oxide electrodes [10,11,13,14]. O'Regan et al. [2] have found that applying an external voltage has a distinct effect on the efficiency of charge separation in dye-sensitised nanoporous TiO_2 electrodes.

It is our objective to study the potential distribution in nanostructured TiO_2 films by means of electrolyte electroreflection (EER). This in situ technique has proven to be a valuable tool in semiconductor electrochemistry. It has been used to study the band structure [15], to determine the potential distribution between the space charge and Helmholtz layer [16], to identify surface states [17,18], and to obtain flat-band potentials [18–23]. In EER, a periodically modulated electric field is applied to the semiconductor electrode, which causes small changes in the reflectivity and the absorbance. When the modulated electric field is sufficiently low, a relatively simple electroreflectance spectrum is obtained upon scanning the wavelength. The resulting lineshape is determined by the intrinsic properties of the crystal and is related to the third derivative of the dielectric function. A general theoretical description of electroreflection is given by Aspnes [22].

In addition to EER experiments, the influence of applied potential on photocurrent generation by UV light has also been studied. Marked differences are observed between back and front-side illumination, and between continuous and chopped illumination. In both EER and photocurrent generation, surface states at the TiO_2|electrolyte interface play an important role.

2. Experimental

Porous nanocrystalline TiO_2 electrodes of about 10 μm thickness were prepared from Degussa P25 TiO_2 powder, following a method described by Nazeeruddin et al. [3]. In short, the TiO_2 powder, with a small amount of water and acetylacetone added, was ground in a mortar, and diluted with water to obtain a white, viscous paste. After addition of some Triton X100, the paste was spread onto indium tin oxide- (ITO) coated glass substrates (Glastron, 30 Ω/□). The thickness of the ITO coating is approximately 80 nm. The dried samples were heated for 1 h at 450°C in air. The resulting films were white and highly light scattering, but smooth as was judged from the shiny reflecting surface. In addition, a Nb-doped TiO_2 single crystal (rutile, $N_D \approx 10^{17}\,cm^{-3}$) with the (100) plane exposed was used as a reference system. This crystal was polished mechanically to obtain a mirror-like surface. At the backside, an ohmic contact was made using indium, to which conducting wires were attached using silver paint. Except for the front face, the whole crystal was embedded in epoxy.

The electrochemical cell consisted of a 2 cm pathlength optical glass cuvette, with a Pt counter electrode, a saturated calomel electrode (SCE) reference, and a nanostructured TiO_2 working electrode. A geometrical area of 0.7 cm^2 of the working electrode was exposed to the electrolyte. An aqueous solution of 0.1 M $KClO_4$, acidified to pH 3 using $HClO_4$, served as electrolyte. The solution was deaerated by purging with N_2 before and during the experiments.

The EER set-up consisted of a 150 W xenon lamp with a monochromator (0.275 m, Acton Research Company), potentiostat (Schlumberger Solartron ECI Model 1286), photomultiplier, digital multimeter (Keithley Model 2001), and a lock-in amplifier (EG&G Model 5210 or Stanford Research Systems Model 850 DSP). The internal oscillator of the lock-in amplifier provided the frequency-modulated voltage to the potentiostat. The light incidence on the electrode was close to normal; the reflected light was directed to a photomultiplier via a quartz fibre. The output of the photomultiplier was measured as a voltage drop over a 1000 Ω high-precision resistor by the multimeter and by the lock-in amplifier, to obtain the constant and the voltage-modulated reflectance signals respectively. The set-up was controlled by a PC with an IEEE-488 interface. Steady state photocurrent–potential characteristics were recorded using the same light source and potentiostat. In addition, the lock-in amplifier was used to record photocurrent–potential curves with light that was chopped at a frequency of 3 Hz using a Uniblitz electronic shutter.

3. Results

3.1. EER

In order to check the validity and accuracy of the EER set-up, first the response of single-crystalline TiO_2 was measured. The resulting EER spectrum exhibits a broad peak at 4.0 eV (Fig. 1(a)). The shape of the curve is very similar to those reported by Vos and Krusemeyer [23] and Salvador and co-workers [19,20]. The amplitude and the phase of the EER signal are dependent on the applied d.c.-potential. In Fig. 1(b) this dependency is shown, using 310 nm light. At a potential of −0.41 V vs. SCE the $\Delta R/R$-signal goes through zero, indicating the position of the flat-band potential V_{fb} [20,21]. This value is in accordance with V_{fb} values obtained by EER of −0.36 V for a TiO_2 single crystal reduced in hydrogen [19,20]. Finklea [9] reported that 187 published V_{fb}-values for TiO_2, obtained by the more commonly used Mott–Schottky and

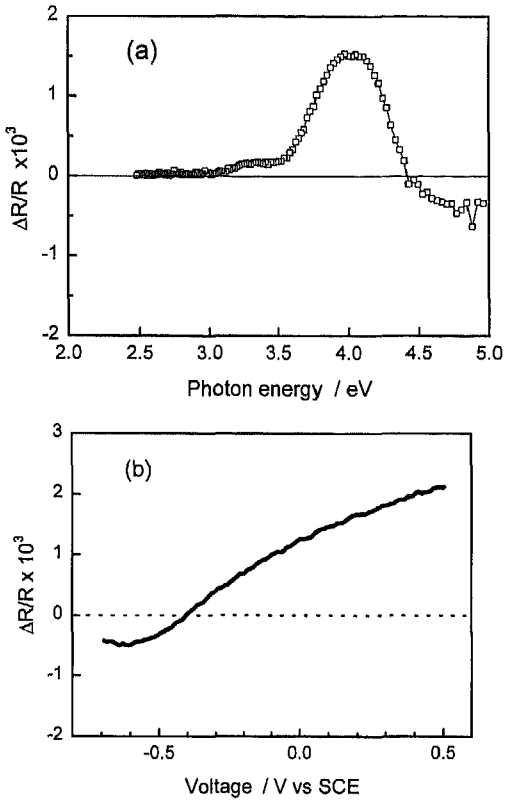

Fig. 1. EER of a Nb-doped TiO_2 single crystal in 0.1 M $KClO_4$ electrolyte (pH 3). (a) EER spectrum at $V_{dc} = 0.5$ V vs. SCE. The modulating voltage was 200 mV r.m.s., and the frequency 120 Hz. (b) Dependence of $\Delta R/R$ on applied d.c.-voltage for a Nb-doped TiO_2 single crystal with $\lambda = 310$ nm.

photocurrent-onset methods, are spread around −0.42 V vs. SCE at pH 3.

The uncoated ITO support gives rise to an EER signal as well, which is expected since ITO is a degenerate semiconductor. In Fig. 2(a) EER spectra of a bare ITO electrode annealed at 450°C are given. For both front- and back-side irradiation, a clear structure at about 2.9 eV is observed. At photon energies larger than 3.5 eV the spectra for front- and back-side irradiation start to differ significantly. The EER spectra of ITO are not sensitive to the applied d.c.-voltage. In Fig. 2(b) spectra recorded at 0.5 and −0.5 V vs. SCE are shown. At both potentials the shape as well as the amplitude of the EER spectra are identical.

For porous nanocrystalline TiO_2 electrodes the EER response is strongly dependent on the direction of illumination. When front-side illumination is used, only with sub-bandgap light is an EER response found (Fig. 3(a)). This response is relatively weak and is strongly dependent on the frequency of the voltage modulation. At high frequencies of 80 Hz or higher no significant EER signal can be detected, whereas at lower frequencies a clear response is observed. The shape of the EER spectrum is essentially featureless and independent of the applied d.c.-voltage. The amplitude of the EER signal increases markedly at potentials negative to 0 V (Fig. 3(a) and Fig. 3(b)). When the potential is scanned from positive to negative, a maximum $\Delta R/R$-response at 500 nm is observed at about −0.45 V (Fig. 3(b)).

Irradiation through the back-side, i.e. through the ITO support, leads to very different EER spectra. In Fig. 4(a) EER spectra recorded at different d.c.-voltages are shown. A broad response round 3.4 eV is observed. The shape of the curves is independent of the applied bias voltage, but at −0.4 V vs. SCE the $\Delta R/R$ signal is much smaller than at more positive potentials. At −1.0 V, no EER signals are found at all. The dependence of $\Delta R/R$, monitored at a single wavelength (360 nm), as a function of d.c.-potential is shown in Fig. 4(b). When the potential is scanned in the negative direction, the signal decreases sharply between −0.2 and −0.4 V. The signal approaches zero at −0.5 V vs. SCE. There is, however, no zero-crossing and concomitant sign reversal. The $\Delta R/R$ value at 3.4 eV is linearly dependent on the applied modulation amplitude in a range of 10 to 400 mV. In contrast to front-side EER, the frequency of the voltage modulation (100 to 1 Hz) has no marked effect on the amplitude of the $\Delta R/R$-signal. Also, the shape of the EER spectrum does not change with frequency.

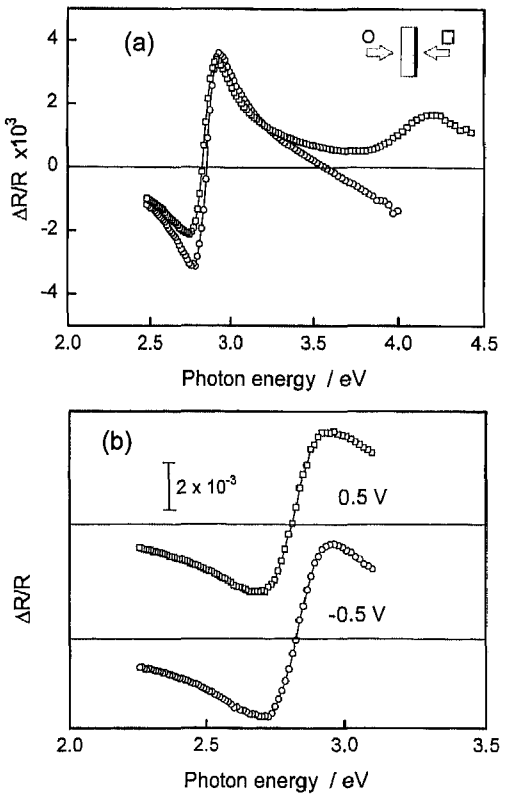

Fig. 2. EER spectra of ITO, annealed at 450°C. (a) EER spectra, using front-side (□) and back-side irradiation (○). In back-side irradiation, light is incident on the glass side of the ITO electrode. $V_{ac} = 200$ mV r.m.s., frequency 120 Hz. The d.c. bias voltage was 0.5 V vs. SCE. (b) EER spectra recorded at 0.5 and −0.5 V vs. SCE. $V_{ac} = 100$ mV r.m.s., frequency 80 Hz.

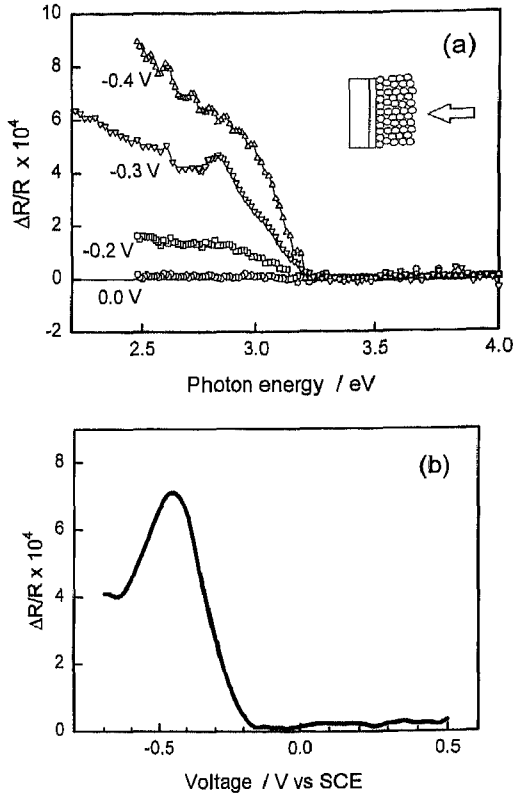

Fig. 3. EER of a porous nanocrystalline TiO_2 film deposited on an ITO support. Front-side illumination is used, with the light falling directly on the porous TiO_2 film. $V_{ac} = 100$ mV r.m.s., frequency 10 Hz. (a) EER spectra recorded at different d.c.-voltages (indicated in the figure). (b) Dependence of $\Delta R/R$ on applied d.c.-voltage. The irradiation wavelength is 500 nm (2.48 eV). The voltage is scanned from 0.5 to −0.7 V vs. SCE with a scan rate of 5 mV s^{-1}.

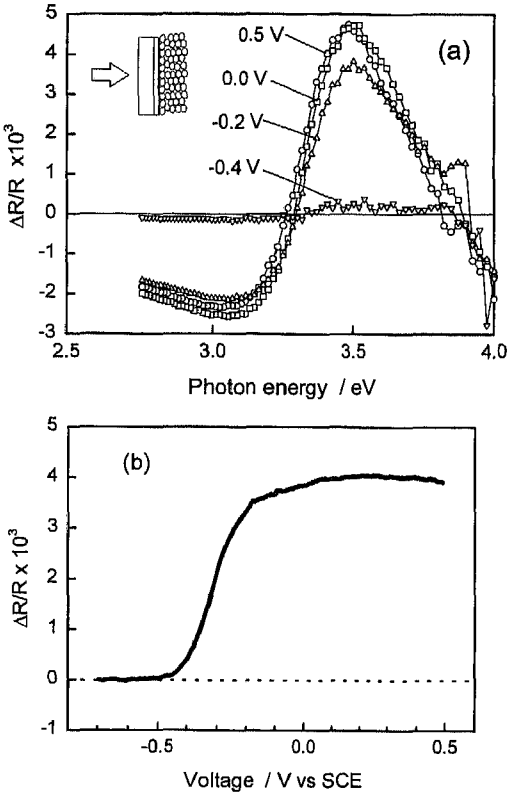

Fig. 4. EER of a porous nanocrystalline TiO_2 film deposited on an ITO support using back-side illumination (i.e. through the ITO support). $V_{ac} = 100$ mV r.m.s., frequency 80 Hz. (a) EER spectra recorded at different d.c.-voltages, indicated in the figure. (b) Dependence of $\Delta R/R$ on applied d.c.-voltage; voltage scan from 0.5 to −0.7 V vs. SCE with a scan rate of 5 mV s^{-1}, using 360 nm (3.44 eV) illumination.

3.2. Potential dependence of photocurrents

UV irradiation of nanostructured TiO_2 electrodes leads to the generation of anodic photocurrents. The contribution of the ITO substrate to the photocurrent is negligible. Fig. 5 shows the current–potential characteristics of a porous nanocrystalline TiO_2 electrode in the dark and upon continuous 350 nm illumination. The difference between the light and the dark curve, i.e. the photocurrent, is practically independent of the applied voltage at potentials positive of 0 V vs. SCE. This behaviour is independent of the side of illumination. Back-side illumination results in two times higher photocurrents than front-side illumination. The IPCEs are 27% and 13% for back and front-side illumination respectively.

The photocurrent response to chopped irradiation is markedly different. In Fig. 6 photocurrents detected by a lock-in amplifier are shown as a function of the applied potential. The incident light (350 nm) is chopped at a frequency of 3 Hz. With back-side irradiation the magnitude of the alternating-photocurrent is comparable to that of direct-photocurrent upon continuous irradiation. There is, however, a certain voltage dependence of the photocurrent. With front-side irradiation, no alternating-photocurrents are observed at potentials positive of 0 V; only at around −0.35 V vs. SCE is some photocurrent response found. In this experiment a direct current is measured that

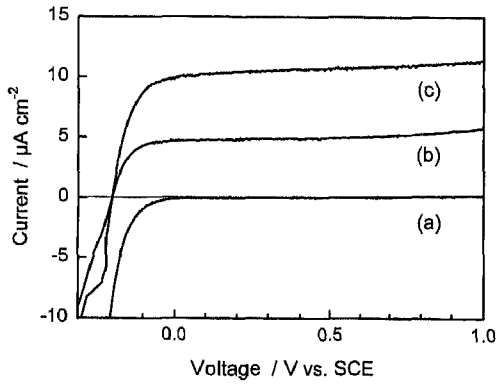

Fig. 5. Current–potential characteristics of a nanostructured TiO_2 electrode in 0.1 M $KClO_4$ aqueous electrolyte (pH3, N_2-purged). (a) In the dark, (b) front-side illumination, (c) back-side illumination. The light has a wavelength of 350 nm and an intensity of 0.15 mW cm^{-2}. The voltage is scanned from positive to negative potentials at a rate of 5 mV s^{-1}.

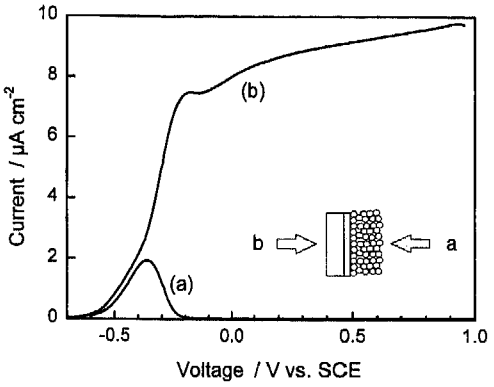

Fig. 6. Potential-dependence of the 3 Hz alternating-photocurrent of a porous nanocrystalline TiO_2 electrode, as measured with the lock-in technique. (a) Front-side illumination, (b) back-side illumination. The conditions are similar to Fig. 6, except that the light beam is chopped at a frequency of 3 Hz.

lies halfway between the dark current and the current found under steady-state illumination.

4. Discussion

4.1. EER

The lineshape of a third derivative EER spectrum has the following general form [22]

$$\Delta R/R = Re\left[C\,e^{i\theta}\left(E - E_g + i\Gamma\right)^{-n}\right] \quad (1)$$

where C and θ are the amplitude and phase factors, E_g is the energy of a critical point, Γ is the broadening parameter, and n is 3 or 2.5 for a two- or three-dimensional parabolic critical point model respectively. A critical point, for instance a direct optical transition, gives rise to one minimum and one maximum in the EER spectrum. The energy of the optical transition is located somewhere in between, depending on the relative intensities of the peaks. By using a graphical method E_g and Γ can easily be determined [22]. The magnitude of the $\Delta R/R$ signal is dependent on the electric field strength in the material near the surface E_s [24,25]:

$$\Delta R/R = L(h\nu)\,E_s^2 \quad (2)$$

where $L(h\nu)$ is the wavelength-dependent lineshape factor. When the penetration depth of the light is smaller than the depletion layer of the semiconductor electrode, it can be shown that a linear relationship between $\Delta R/R$ and the applied potential holds [16].

The electroreflection spectrum of the Nb-doped TiO_2 single crystal has a critical energy point at 4.1 eV and a broadening factor of 0.7 eV. This critical point corresponds to a direct optical transition of rutile at this energy. The 180° EER phase shift at −0.41 V vs. SCE indicates a change in direction of the electric field at the semiconductor|electrolyte interface. Depletion exists at potentials positive to the cross-over point, while accumulation is present at more negative potentials. Salvador and co-workers [19–21] have shown that the potential where the phase of the EER signal amplitude shifts 180° and the amplitude goes to zero is a good measure of the flat-band potential.

EER spectra of bare ITO substrates (Fig. 2(a)) show a clear response around 2.9 eV. This energy coincides with the reported indirect bandgap of polycrystalline In_2O_3 of 2.8 eV [26]. This coincidence is remarkable, since it is generally accepted that indirect transitions do not give rise to EER signals. It should be noted, however, that the EER response is independent of the applied d.c.-potential (Fig. 2(b)), which indicates that conventional low-field electroreflectance does not occur. ITO is a degenerate semiconductor with a donor density of $10^{20}\,cm^{-3}$.[1] At 1 V band bending, the thickness of the space-charge layer is only about 2 nm. Electric field strengths of ca. $5 \times 10^8\,V\,m^{-1}$ are present at the ITO|electrolyte interface, which is outside the low-field regime [22]. It should also be noted that reported bandgaps of ITO, i.e. $In_{2-x}Sn_xO_3$ with $x \approx 0.2$, differ from that of stoichiometric In_2O_3 [28]. Unambiguous assignment of the nature of the optical threshold of ITO is, therefore, problematic. Further investigation of opto-electronic properties of ITO is required, but this task lies beyond the scope of this paper.

When a nanostructured TiO_2 film is deposited onto an ITO support, both front- and back-side irradiation EER-spectra differ clearly from those of the uncoated ITO (compare Fig. 3(a) and Fig. 4(a) with Fig. 2(a)). Furthermore, $\Delta R/R$-signals show a clear dependence on the bias potential (Fig. 3(b) and Fig. 4(b)), in contrast to those of the bare ITO electrode (Fig. 2(b)). Hence, the EER response is essentially caused by the nanoporous TiO_2 film. Front- and back-side EER of porous nanocrystalline TiO_2 electrodes leads to totally different spectra. In order to unravel the nature of the observed EER response, it is important to consider the optical properties of the nanoporous TiO_2 electrode. In this study, highly light-scattering electrodes prepared from Degussa P25 have been used. The specular transmission of light with wavelengths smaller than 500 nm is less than 2%. The TiO_2|ITO and TiO_2|electrolyte interfaces, however, are very smooth and give rise to a considerable specular reflection. Since in our EER-set-up only the specular part of the reflected light is detected, the $\Delta R/R$-signals arise from the TiO_2|electrolyte interface when the front-side irradiation is used and from the TiO_2|ITO interface in case of back-side irradiation.

In case of front-side EER of porous nanocrystalline TiO_2 electrodes, a featureless sub-bandgap response is observed (Fig. 3(a)). The absence of band-to-band re-

[1] Mott–Schottky analysis at 10 kHz of ITO electrodes yielded V_{fb} and N_D of ca. −0.5 V vs. SCE (pH 3) and $10^{20}\,cm^{-3}$ respectively [27].

sponse indicates that the electric field inside the TiO_2 particles that are located at the outside of the film is not affected by the applied modulation voltage. Only negative of 0 V vs. SCE are significant EER signals found. In the same voltage range, in the $j-V$ curve a cathodic current is observed (Fig. 5(a)), corresponding to the transfer of electrons from the ITO substrate to the porous TiO_2 structure rather than a chemical reaction, since this is well below the reduction potential of water (-0.42 V at pH 3). Both conduction band electrons and electrons that are trapped at surface states could cause a sub-bandgap EER response. Modulation of the electrode potential leads to a.c.-perturbation of the surface state population. Sub-bandgap photons are able to empty the surface states and thus respond to the potential perturbation. Bandgap light, however, leads to the formation of electron–hole pairs which diminish the influence of the potential modulation of the reflection. A clear maximum is observed at -0.45 V vs. SCE in the $\Delta R/R$ vs. potential plot (Fig. 3(b)), which indicates the influence of surface states. Once most surface states are filled due to the applied bias voltage, the $\Delta R/R$ signal will start to decrease. Surface states on titanium dioxide have been observed by EER before [17,18]. Due to the very high surface to volume ratio of nanoporous electrodes, EER response of surface states is expected to play an important role in our case. The strong dependence of the observed $\Delta R/R$ signal on the modulation frequencies reflects the slow electron transport and trapping kinetics of the nanoporous TiO_2 electrode.

Back-side irradiation gives rise to an oscillatory EER spectrum in the UV region. This indicates that applied voltage modulation gives rise to an a.c. electric field within the porous TiO_2 film near the ITO support. Nanoporous films are expected to be fully depleted of free charge carriers at potentials positive of the flat-band potential [2,29]. Therefore, the EER signals observed here are not caused by a modulation of the band bending inside the individual TiO_2 particles. Instead, EER response is thought to be caused by electric field modulation across a fraction of the nanoporous TiO_2 film. The porous TiO_2 film is thus regarded as a dielectric rather than a semiconductor surface layer, and can, therefore, sustain a macroscopic electric field that can be modulated externally to give $\Delta R/R$ signals. In contrast to front-side EER, back-side EER response is essentially independent of the modulation frequency in the range of 1 to 100 Hz, which is another aspect of the difference in origin of the EER signals obtained with back- and front-side illumination.

Although the exact nature of EER signals on nanostructured TiO_2 electrode is uncertain, the EER spectrum (back-side irradiation, Fig. 4(a)) can be fitted to Eq. (1), yielding $E_g = 3.3$ eV and $\Gamma = 0.4$ eV. In samples with different annealing temperature and time there is a spread in the critical point energy ($E_g = 3.3$ to 3.7 eV). The nanostructured TiO_2 is composed of Degussa P25, which is a mixture of separate particles of anatase and rutile in a ratio of ca. 70% and ca. 30% respectively [30]. The indirect bandgaps of anatase and rutile have been determined at 3.2 eV and 3.0 eV respectively. In both anatase and rutile direct optical transitions are present at higher energies [31]. Since the dispersion in the measured critical point energy is high (3.3 to 3.7 eV) and dependent on the film preparation conditions, it is difficult to derive an unambiguous assignment. The observed influence of the anneal temperature and time suggests a variation in the film crystallinity. The ratio of anatase to rutile may change. Also, changes in the surface properties of the porous film can account for the spread in the EER spectra.

The applied d.c.-potential does not affect the shape of the EER spectrum for nanoporous TiO_2 (Fig. 4(a)), which is a characteristic of low-field electroreflectance [22]. The potential dependence of EER signals (Fig. 4(b)) indicates the presence of an electric field at the ITO|nanoporous TiO_2 interface under depletion conditions. Starting from 0.5 V vs. SCE, the $\Delta R/R$ signal is initially almost independent of the applied d.c.-voltage. Negative of -0.1 V the EER signal decreases. This can be ascribed to a decrease in electric field strength. However, filling of TiO_2 surface states should also be taken into account, since this occurs in the same voltage range. Filling of surface states by electrons leads to an extra surface charge at the semiconductor|electrolyte interface which may result in unpinning of the band edges of the TiO_2 [14]. This causes additional applied voltages to drop partially in the Helmholtz layer, resulting in smaller EER signals. Negative to -0.5 V vs. SCE no EER signal is observed, which indicates that the applied modulation voltage no longer causes an a.c. potential gradient in the porous TiO_2 film. The absence of any EER signal excludes the formation of an accumulation layer in the colloidal TiO_2 film. An EER signal with 180° phase shift is expected in the case of an accumulation layer, as has been demonstrated with the Nb-doped TiO_2 single crystal (Fig. 1(b)).

Fitzmaurice and co-workers have assumed that an accumulation layer is formed in nanostructured metal oxide electrodes at potentials negative to the flat-band potential [29,32]. In their experiments, the free-electron absorption in nanostructured metal oxide electrodes is monitored as a function of potential. When the electrode is biased close to or negative of the flat-band potential, free electrons in the conduction band as well as electrons trapped in surface states absorb light in the near infra-red region. The increase in near infra-red absorbance is accompanied by a decrease in UV absorbance. These results have been interpreted as evidence for the formation of an accumulation layer. However, intercalation of small ions like H^+ and Li^+ at potentials negative of the flat-band potential [5,14,33], can also account for the observed absorbance behaviour. The intercalated ions act as dopant impurities, hence the donor density of TiO_2 increases when intercalation takes place. The energy distance of the Fermi level with respect to the conduction band minimum reduces as

the dopant concentration increases, and may even shift inside the conduction band, resulting in a degenerate semiconductor. This filling of conduction band energy levels explains the observed absorption loss at wavelengths shorter than that of the fundamental absorption edge.

4.2. Potential dependence of photocurrents

Steady-state photocurrents are almost independent of the applied voltage, at voltages positive of 0 V vs. SCE (Fig. 5). Therefore, in this region the potential applied to the ITO support has practically no influence on the properties of the nanoporous TiO_2 film that affect the efficiency of photocurrent generation, such as the number of electrons in the conduction band, the electron velocity, and the presence of electric fields. It is likely that only inside TiO_2 particles that are in direct contact with the ITO support can an electric field exist that can be modulated externally. These particles can account for the EER signals upon back-side irradiation as well as for the small potential dependence of the photocurrent that is observed upon close examination of Fig. 5. Negative of −0.1 V vs. SCE a cathodic current starts to flow. Transport of electrons from the ITO support to the porous TiO_2 film must take place since at bare ITO electrodes there is almost no current in this potential range. As a result, the density of electrons in the TiO_2 conduction band or trapped in surface states increases and affects the photocurrent generation. At about −0.5 V vs. SCE steady-state photocurrent can no longer be observed, i.e. all the generated electron–hole pairs recombine.

When chopped light and lock-in detection is used to measure the photocurrent–potential dependence a different behaviour is found (Fig. 6). In back-side illumination, the magnitude of the alternating-photocurrent is only slightly smaller than the steady-state (direct) photocurrent. Hence, transport of electrons from the nanoporous TiO_2 film to the ITO substrate can follow the 3 Hz excitation. The penetration depth of 350 nm light in a dense anatase film is about 500 nm [34], and may be even smaller in the nanoporous TiO_2 film due to light-scattering. Therefore, it is not surprising that the response of the electrode is relatively fast. Upon front-side illumination and at voltages larger than 0 V vs. SCE the 3 Hz alternating-photocurrent is almost zero. In contrast, a non-zero direct current is measured by the potentiostat in this experiment, indicating that photocurrent generation does take place. The absence of 3 Hz an alternating-photocurrent signal is due to the slow photocurrent response of nanostructured electrodes. Photo-generated electrons have to travel a relatively long distance (ca. 10 μm) through the porous structure before reaching the ITO support. Trapping and detrapping of electrons will enlarge the travel time greatly. When the electrode is biased closer to the flat-band potential 3 Hz alternating-photocurrents are found with back-side as well as front-side excitation. Apparently, the response time of the electrode is much shorter under these conditions. Polarising the electrode close to the flat-band potential leads to filling of traps in the nanoporous TiO_2 film, resulting in a faster transport of photo-generated electrons. The response time depends clearly on the occupation of electron traps. This conclusion is supported by the observations using intensity-modulated photocurrent spectroscopy as reported elsewhere [35].

5. Conclusions

Back- and front-side EER of porous nanocrystalline TiO_2 electrodes in aqueous indifferent electrolyte leads to entirely different responses. Front-side EER (with light falling directly on top of the TiO_2 film) gives a sub-band-gap EER-response due to surface states. Back-side EER (through the ITO support) gives a band-to-band response, probably due to electric field modulation in TiO_2 particles located at the ITO|TiO_2 interface. Polarising the nanoporous electrode close to the flat-band potential results in filling of surface states, which causes marked effects on the front- and back-side EER signals as well as on the alternating-photocurrent response. These effects occur at potentials negative of −0.1 V vs. SCE (pH 3), indicating that surface states are located ca. 0.4 eV below the conduction band edge. At potentials more than 0.5 V positive of the flat-band potential the steady-state photocurrent generation is essentially independent of the applied voltage.

Acknowledgements

This work was supported by Novem (Netherlands Agency for Energy and the Environment). A.G. acknowledges the Royal Netherlands Academy of Sciences (KNAW) for his fellowship. Dr. D. Meissner (ISFH, Hannover, Germany) is acknowledged for putting a Nb-doped TiO_2 single crystal at our disposal.

References

[1] B. O'Regan and M. Grätzel, Nature, 353 (1991) 737.
[2] B. O'Regan, J. Moser, M. Anderson and M. Grätzel, J. Phys. Chem., 94 (1990) 8720.
[3] M. Nazeeruddin, A. Kay, I. Rodicio, R. Humphry-Baker, E. Müller, P. Liska, N. Vlachopoulos and M. Grätzel, J. Am. Chem. Soc., 115 (1993) 6382.
[4] X. Marguerettaz, R. O'Neill and D. Fitzmaurice, J. Am. Chem. Soc., 116 (1994) 2629.
[5] A. Hagfeldt, N. Vlachopoulos and M. Grätzel, J. Electrochem. Soc., 141 (1994) L83.
[6] D. Liu and P.V. Kamat, J. Electrochem. Soc., 142 (1995) 835.
[7] S.Y. Huang, L. Kavan and M. Grätzel, J. Electrochem. Soc., 142 (1995) L142.
[8] S.R. Morrison, Electrochemistry at Semiconductor and Oxidized Metal Electrodes, Plenum, New York, 1980.

[9] H.O. Finklea, Semiconductor Electrodes, Elsevier, New York, 1988.
[10] A. Hagfeldt, U. Björkstén and S.-E. Lindquist, Sol. Energy Mater. Sol. Cells, 27 (1992) 293.
[11] U. Björkstén, J. Moser and M. Grätzel, Chem. Mater., 6 (1994) 858.
[12] S. Södergren, A. Hagfeldt, J. Olssen and S.-E. Lindquist, J. Phys. Chem., 98 (1994) 5552.
[13] A. Hagfeldt, S.-E. Lindquist and M. Grätzel, Sol. Energy Mater. Sol. Cells, 32 (1994) 245.
[14] F. Cao, G. Oskam, P.C. Searson, J.M. Stipkala, T.A. Heimer, F. Farzad and G.J. Meyer, J. Phys. Chem., 99 (1995) 11974.
[15] W. Cardona, Modulation Spectroscopy, Solid State Physics Supplement 11, Academic Press, New York, 1969.
[16] G.A. Scholtz and H. Gerischer, J. Electrochem. Soc., 132 (1985) 1643.
[17] W. Siripala and M. Tomkiewicz, Phys. Rev. Lett., 50 (1983) 443.
[18] I.J. Ferrer, H. Muraki and P. Salvador, J. Phys. Chem., 90 (1986) 2805.
[19] J. Gandia, M. Pujadas and P. Salvador, J. Electroanal. Chem., 244 (1988) 69.
[20] M. Pujadas and P. Salvador, J. Electrochem. Soc., 136 (1989) 716.
[21] P. Salvador, J. Electrochim. Acta, 37 (1992) 957.
[22] D.E. Aspnes, Surf. Sci., 37 (1973) 418.
[23] K. Vos and H.J. Krusemeyer, J. Phys. C:, 10 (1977) 3893.
[24] D.E. Aspnes and J.E. Rowe, Solid State Commun., 8 (1970) 1145.
[25] D.E. Aspnes, Phys. Rev. Lett., 28 (1972) 913.
[26] L.C. Schumacher, S. Mamiche-Afara and M.J. Dignam, J. Electrochem. Soc., 133 (1986) 716.
[27] G.K Boschloo, unpublished results.
[28] J.E.A.M. van den Meerakker, E.A. Meulenkamp and M. Scholten, J. Appl. Phys., 74 (1993) 3282.
[29] G. Rothenberger, D. Fitzmaurice and M. Grätzel, J. Phys. Chem., 96 (1992) 5983.
[30] A.K. Datye, G. Riegel, J.R. Bolton, M. Huang and M.R. Prairie, J. Solid State Chem., 115 (1995) 236.
[31] N. Daude, C. Gout and C. Jouanin, Phys. Rev. B:, 15 (1977) 3229.
[32] G. Redmond and D. Fitzmaurice, J. Phys. Chem., 97 (1993) 1426.
[33] L.A. Lyon and J.T. Hupp, J. Phys. Chem., 99 (1995) 15718.
[34] G.K. Boschloo, A. Goossens and J. Schoonman, submitted to J. Electrochem. Soc.
[35] G.K. Boschloo and A. Goossens, in preparation.